ACS Infectious Diseases

Article

Cite This: ACS Infect. Dis. 2018, 4, 936−943

pubs.acs.org/journal/aidcbc

A Highly Dynamic Loop of the *Pseudomonas aeruginosa* PA14 Type IV Pilin Is Essential for Pilus Assembly

Ylan Nguyen,[†,‡] Stephen Boulton,[§] E. Tyler McNicholl,[§] Madoka Akimoto,[§] Hanjeong Harvey,[†,‡] Francisca Aidoo,[†,‡] Giuseppe Melacini,[†,§] and Lori L. Burrows*[,†,‡]

[†]Department of Biochemistry and Biomedical Sciences, [‡]Michael G. DeGroote Institute for Infectious Disease Research, and [§]Department of Chemistry, McMaster University, 1280 Main Street West, Hamilton, Ontario L8S 4K1, Canada

ABSTRACT: Type IVa pili (T4aP) are long, thin surface filaments involved in attachment, motility, biofilm formation, and DNA uptake. They are important virulence factors for many bacteria, including *Pseudomonas aeruginosa*, an opportunistic pathogen and common cause of hospital-acquired infections. Each helical filament contains thousands of monomers of the major pilin subunit, PilA. Each *P. aeruginosa* strain expresses one of five phylogenetically distinct major pilins, which vary in sequence and the nature of their associated accessory protein(s). Here, we present the backbone resonance assignment of the C-terminal domain of the group III PilA from strain PA14, a highly virulent, globally distributed clone. Secondary structure probabilities calculated from chemical shifts were in excellent agreement with previous homology modeling using a group V pilin structural template. The analysis revealed that the distal segment of the $\alpha\beta$ loop had high microsecond−millisecond dynamics compared with other loop regions. Shortening of this segment by internal deletion abrogated pilus assembly in a dominant negative manner, suggesting a potential role in pilin polymerization. Pilin conformations that support optimal interactions of both the conserved hydrophobic N-termini in the pilus core and hydrophilic loops creating the filament surface may be necessary to produce stable filaments.

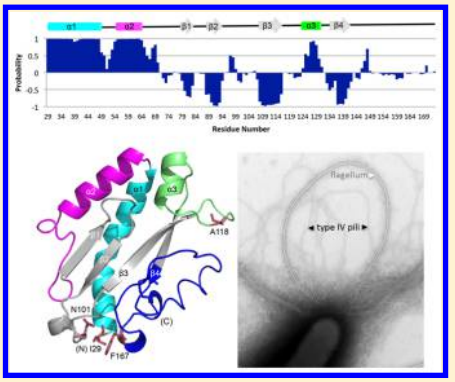

KEYWORDS: *Type IV pili, pilin, nuclear magnetic resonance, Pseudomonas aeruginosa, PilA, dynamics*

Type IV pili (T4P) are dynamic, multifunctional protein filaments that are strong enough to withstand piconewton-scale forces, equivalent to 100 000 times the body weight of a bacterial cell, yet can be reversibly assembled and disassembled at a rate of a thousand subunits per second. The specific protein−protein interactions that allow for these properties are not well understood. T4P are expressed by a wide range of bacteria and archaea, including *Pseudomonas aeruginosa*, *Neisseria spp.*, *Vibrio cholerae*, *Clostridium perfringens*, and *Methanococcus maripaludis*.[1−3] They are involved primarily in attachment to and "twitching" motility along surfaces but also contribute to biofilm formation, bacteriophage adsorption, uptake of extracellular DNA, and electron transfer to external acceptors.[3,4] They are generally divided into two subfamilies (T4aP and T4bP) based on distinctive features of the pilin subunits and components of the assembly systems.[5] The T4aP subfamily is typically associated with twitching motility, which involves repeated rounds of pilus assembly, adherence, and disassembly, pulling the cells forward in a grappling hook-like manner.

T4aPs are an important virulence factor for the opportunistic pathogen, *P. aeruginosa*, which infects HIV, cancer, and burn patients and causes chronic lung infections in people with cystic fibrosis, contributing to morbidity and mortality.[6,7] It is a common cause of hospital-acquired infections that, due to its intrinsic antibiotic resistance and ability to form biofilms, are difficult to treat. *P. aeruginosa* uses its T4aP to initiate infection via host attachment and invasion and to colonize abiotic surfaces such as medical devices and contact lenses.[8] Loss of T4aP, or T4aP retraction, impairs *P. aeruginosa* virulence,[9] making them potential therapeutic targets.

P. aeruginosa T4aPs are composed of thousands of copies of a single protein, the major pilin PilA, plus small amounts of minor pilins, and the adhesin PilY1 that primes pilus assembly.[10−12] Pilins are translated as prepilins and processed on the cytoplasmic face of the inner membrane by a prepilin peptidase into 15−18 kDa mature pilins prior to assembly.[13] As surface-exposed components, pilins are potential vaccine candidates, but a clearer understanding of the spectrum of their structural diversity is needed for the rational development of a broadly protective pilin-based vaccine. Each *P. aeruginosa* strain encodes one of five groups of phylogenetically distinct major pilins.[14] The five groups (I−V) are distinguished by pilin sequence, size, and the presence or absence (in the case of group II) of specific accessory protein genes located immediately downstream of the pilin gene.[14] Group I pilins are glycosylated at the C-terminus with a lipopolysaccharide O-antigen unit by their cognate glycosyltransferase TfpO, while group IV pilins are modified on multiple Ser and Thr residues

Received: November 13, 2017
Published: January 17, 2018

DOI: 10.1021/acsinfecdis.7b00229
ACS Infect. Dis. 2018, 4, 936−943

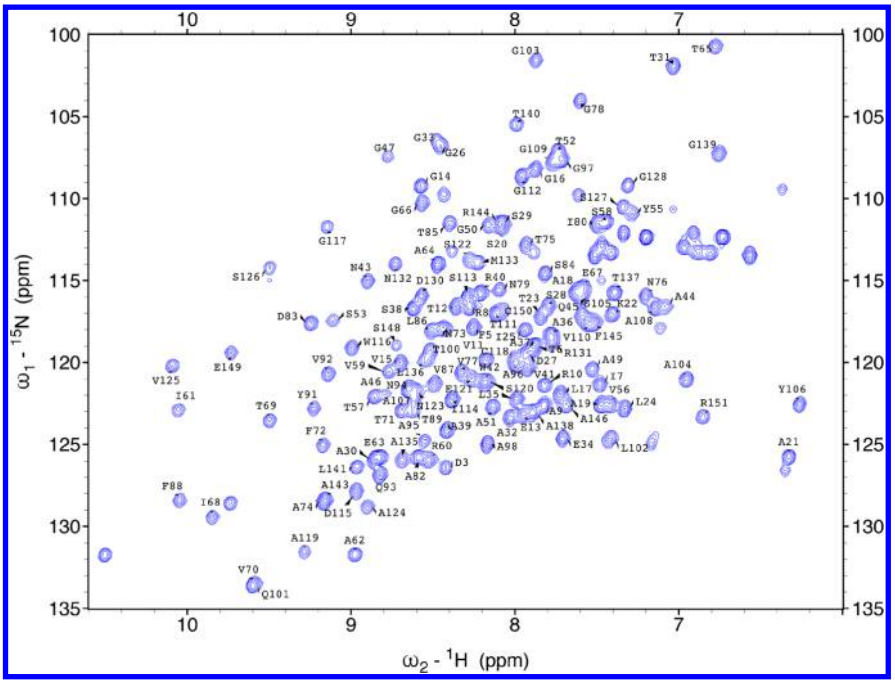

Figure 1. $PilA_{PA14}$ backbone assignment and secondary structure. The 700 MHz ^{15}N-^{1}H-HSQC of ^{13}C and ^{15}N-labeled $PilA_{PA14}$ with residues 1−28 truncated from the mature pilin. Peak assignments for backbone amide N−H atoms are labeled on the basis of residue type and numbered according to the recombinant protein analyzed in the experiment.

with polymers of α1,5-linked D-arabinofuranose by the glycosyltransferase TfpW. These decorations can block the attachment of bacteriophages that use T4aP as receptors.[15] Although group III and V pilins are not post-translationally modified, their accessory proteins TfpY and TfpZ optimize their assembly in an unknown manner.[16] Group I, II, and III pilins are the most common types among *P. aeruginosa* strains.[14] Many studies of T4aP function focus on laboratory strains PAO1, PAK, or PA103, all of which express group II pilins,[17−20] while others use PA14, one of the most frequently isolated clones of *P. aeruginosa* in the world and popular for virulence studies due its pathogenicity toward a variety of host species.[21]

X-ray crystal structures of full length and N-terminally truncated versions of group II pilins from strains PAK and K122-4 were solved by multiple groups.[17−19,22] Their architecture resembles a ladle, with an extended N-terminal α-helix and a globular C-terminal domain. The hydrophobic N-terminal half of the α-helix (α1-N) protrudes from the C-terminal domain, embeds pilins in the inner membrane prior to assembly, and forms the hydrophobic core of the pilus when subunits are polymerized into a filament.[18] To facilitate structural studies, this segment of the protein is frequently removed to increase solubility, as that deletion does not affect folding. The C-terminal domain consists of α1-C packed against a four-stranded antiparallel β-sheet, although the number of strands can vary. The αβ-loop region between α1C and β1, the loops between the β-strands, and the C-terminal disulfide bonded loop are variable in sequence and contribute to the extensive structural diversity of pilin proteins.[23]

We previously solved the X-ray crystal structure of the type IV pilin from group V strain Pa110594,[24] and while it had a conserved pilin fold, there were significant differences in its variable regions compared to group II pilin structures. We also expressed and purified the group III pilin from strain PA14. Even though the protein expressed well and was soluble and monodisperse, it failed to form diffraction-quality crystals. The C-terminal domains of group III and V pilins, excluding the N-terminal 28 residues that are highly conserved in all pilins, share ∼43% identity. Therefore, we generated a homology model of the PA14 pilin using the group V structure as a template, which suggested that divergent residues were mainly located in surface-exposed loop regions.[24]

Here, we used NMR spectroscopy to determine the pilin's secondary structure probabilities based on chemical shifts and to characterize its dynamics. The NMR data were in excellent agreement with the model, showing the pronounced similarity between the underlying architectures of group III and V pilins. Relaxation analyses revealed that a region of the αβ loop was highly dynamic (ms−μs), a property that facilitates protein−protein interactions. Our subsequent genetic and functional studies showed that this segment was important for stable pilus assembly, as shortening it resulted in pilins that were unable to assemble on their own and disrupted assembly in wild type backgrounds in a dominant negative manner.

RESULTS AND DISCUSSION

Validation of a PA14 Pilin Structural Model by NMR Analysis. High quality NMR spectra were collected for the soluble C-terminal domain of $PilA_{PA14}$ (Figure 1). HN, N, C′, Cα, and Cβ backbone assignment of $PilA_{PA14}$ residues were initially attempted using ^{15}N-^{1}H-HSQC, HN(CO)CA, HNCACB, and CBCA(CO)NH data, with ^{15}N-^{1}H-HSQC spectra collected from a leucine-selective ^{15}N-labeled sample. Additional HNCO, HN(CA)CO, and ^{15}N NOESY-HSQC data were collected to facilitate the assignment. Backbone resonances were assigned to 97% of residues (Figure 1). G1 and I2 could not be assigned; however, these residues are artifacts of affinity tag cleavage, rather than native residues of $PilA_{PA14}$. N48, K54 amide N−H atoms, and S148 Cβ were not

DOI: 10.1021/acsinfecdis.7b00229
ACS Infect. Dis. 2018, 4, 936−943

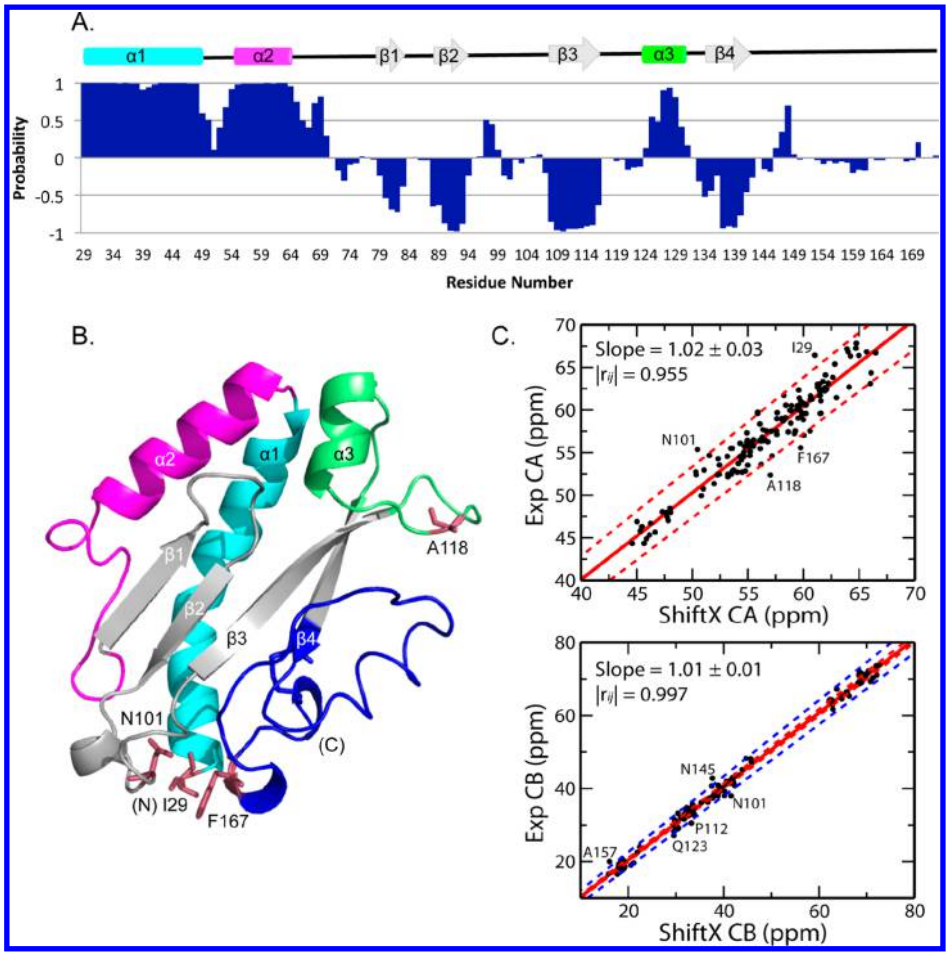

Figure 2. Secondary structure probabilities and comparison of experimental vs. theoretical chemical shifts for CA and CB. (A) Secondary structure probabilities based on chemical shifts are plotted against residue number of the native full-length mature protein. Positive values indicate the residue is in an α-helix, while negative values indicate the residue is a part of a β-strand. The predicted secondary structure is depicted above the plot with α-helices as cylinders and β-strands as arrows. (B) Homology model of the N-terminally truncated $PilA_{PA14}$, showing the secondary structure elements colored as in panel A. The α1-C helix is in cyan; the $\alpha\beta$ loop is magenta; the 4-stranded antiparallel β-sheet is gray; the disulfide-bonded loop is blue. (C) The computed chemical shifts were calculated on the basis of the $PilA_{PA14}$ homology model using the ShiftX server.[28] The calculated CA and CB chemical shifts were then plotted against the chemical shifts measured through triple resonance experiments. Residues that deviated from the line-of-best-fit were labeled in the plots and indicated in burgundy on the homology model in panel B. The dashed red lines in the top panel were computed starting from the line of best fit of the experimental vs ShiftX CA ppm values and adding or subtracting the errors associated with the slope and the y-intercept. The dashed blue lines in the bottom panel were computed similarly, except for the CB ppm correlation, as explained in the Methods section. In each panel, outliers fall outside the range defined by the two dashed lines.

assigned. Chemical shifts were deposited to BioMagResBank (http://www.bmrb.wisc.edu), accession code 26969.

Secondary-structure predictions using protein energetic conformational analysis from NMR chemical shifts (PECAN)[25] (Figure 2A) suggested that the C-terminal domain of $PilA_{PA14}$ contains two N-terminal α-helices followed by four β-strands, with short helices between β2/3 and β3/4 and after β4. The Cβ chemical shifts of C118, 47.3 ppm, and C150, 48.2 ppm (corresponding to C140 and C172 in the full-length mature $PilA_{PA14}$), suggested that these residues participate in a disulfide bond.[26] This predicted secondary structure was consistent with the conserved fold of type IV pilins and agreed well with the homology model of $PilA_{PA14}$ (Figure 2B) predicted using the Phyre2 server using a group V $PilA_{0594}$ structural template.[24,27]

Theoretical Cα and Cβ chemical shifts were computed using the ShiftX Server (http://shiftx.wishartlab.com/),[28] starting from the homology model of the $PilA_{PA14}$ monomer and compared to experimentally measured CA and CB chemical shifts (Figure 2C). CA and CB chemical shifts were explicitly chosen for this comparison since they are sensitive to local dihedral angles and excellent reporters of secondary structure.[29] The ShiftX-predicted chemical shifts were then plotted against the Cα and Cβ chemical shifts measured through triple resonance experiments for protein backbone assignment (e.g., CBCACONH and HNCACB) (Figure 2C). Overall, we observed excellent agreement between the computed and measured chemical shift values, supporting the validity of our PilA model. The data were consistent with the B-factor data published for the related group V $PilA_{0594}$ pilin that was solved by X-ray crystallography, in that regions with higher B-factors in $PilA_{0594}$[24] are highly dynamic in $PilA_{PA14}$. Both pilins have flexible loop regions that are predicted to be involved in subunit−subunit interactions in the pilus fiber, although the sequences in these regions diverge. Outliers were detected by plotting lines obtained from the line of best fit and adding or subtracting the corresponding errors from the slope and y-intercept. Since the slope and intercept errors in the line of best

DOI: 10.1021/acsinfecdis.7b00229
ACS Infect. Dis. 2018, 4, 936−943

fit obtained for the correlation of theoretical and experimental CB chemical shifts were significantly smaller than those for the CA chemical shifts, we conservatively opted to use the errors from the CA correlation. The residues that deviated from the line-of-best-fit were mapped onto the homology model (Figure 2B,C). In general, these residues clustered near the N-terminus of the truncated monomer, with the exception of A118, located in the large insertion in the β3/4 loop.

NMR spin relaxation data were acquired as an indirect validation of the homology model and to probe for significant dynamics in regions that could be important for PilA assembly or filament stability. Several residues (e.g., 49−50, 101−102, 116−120, and 129−131, Figure 3A−C) exhibited fast (ps−ns)

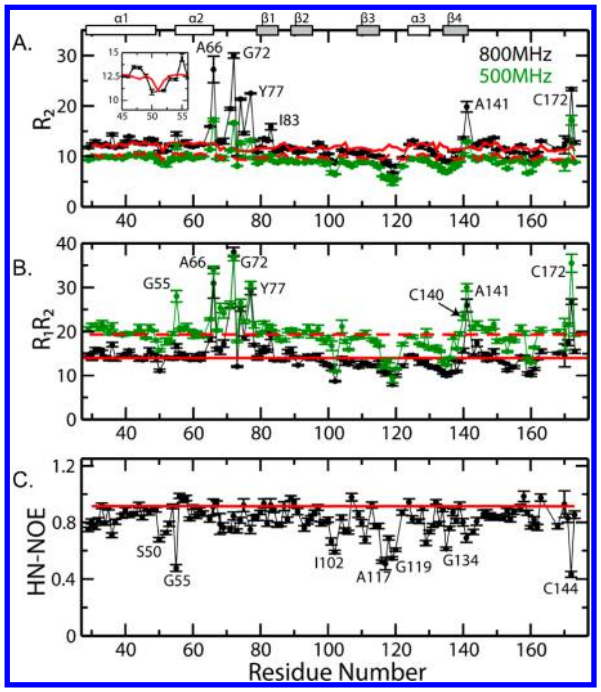

Figure 3. Relaxation analysis of PilA. (A) PilA R_2 relaxation rates were measured at 800 MHz (black) and 500 MHz (green) and compared to the HydroNMR[41] simulated relaxation rates for the PilA homology model at the same field strengths (solid and dashed red lines, respectively). The inset shows the experimental and theoretical R_2 relaxation rates in a representative loop region with fast dynamics. (B) The R_1R_2 product was also computed to minimize contributions arising from the diffusional anisotropy of the overall tumbling. The color coding is the same as in panel A. (C) Heteronuclear $\{^{15}N\text{-}^{1}H\}$ NOEs were also measured to probe fast (ps−ns) dynamics in PilA.

motion, while residues 55, 64−78 in the $\alpha\beta$ loop, 140, 141, and 172 are subject to slower μs−ms dynamics often associated with regions involved in protein−protein interactions, chemical exchange processes, and concerted internal motions.[30] We also computed reduced spectral densities of PilA from R1 and R2 values, as well as heteronuclear $\{^{1}H\text{-}^{15}N\}$-NOEs (HN-NOEs) (Figure 4A−C).

The HN-NOE analysis identified several residues (e.g., ∼50−55, 101−102, 116−120, 129−131, and 172, Figures 3 and 4) subject to local ps−ns motions. These regions all coincide with loops and coils as indicated by the PilA homology model and PECAN analysis shown in Figure 2A,B. However, not all loops and coils displayed significantly enhanced ps−ns dynamics (e.g., the α2-β1 loop and the region following the β4 strand). This does not necessarily indicate a flaw with the homology

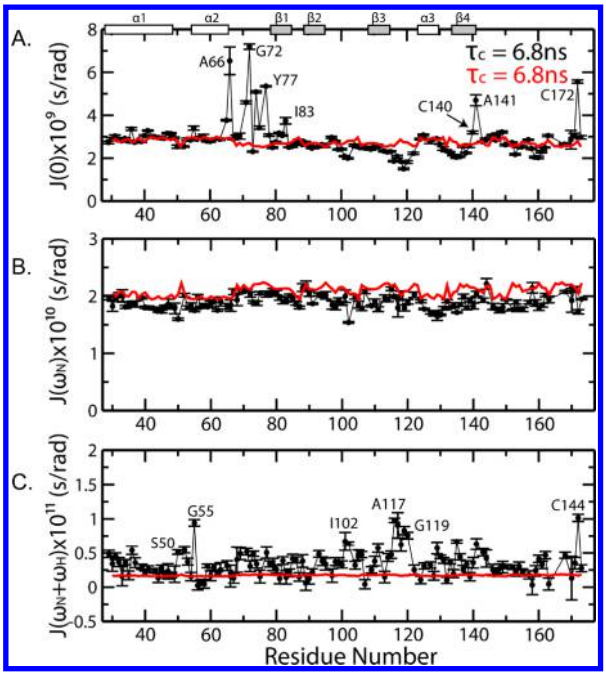

Figure 4. Reduced spectral densities of PilA. (A−C) The black circles denote the reduced spectral densities computed at 0, ω_N, and ω_H ω_N frequencies from the R_1 and R_2 values, as well as the heteronuclear $\{^{1}H\text{-}^{15}N\}$-NOEs (HN-NOEs). The red lines depict the respective reduced spectral densities calculated from the HydroNMR simulated relaxation parameters. PilA's correlation time (τ_c) was derived from the average $J(0)$ value (black) and compared to the τ_c predicted from HydroNMR (red) for the PilA homology model, showing excellent agreement.

model, as there can be other interactions between these regions and the rest of the protein that quench ps−ns dynamics. For instance, the disulfide bridge between C140 and C172 may stabilize the C-terminus and the β4-strand.

Slow (μs−ms) dynamics were also probed through examination of R_2 rates, the R_1R_2 product, and the reduced spectral density function, $J(0)$. The global $J(0)$ rate of residues devoid of any significant ps−ns or μs−ms dynamics is useful to calculate the protein's correlation time (τ_c), which provides information about its overall shape and size. We compared the τ_c of PilA calculated from global averaged $J(0)$ values with the τ_c predicted from HydroNMR simulation of the PilA homology model (Figure 4A) and found they were in excellent agreement. We examined site-specific changes in R_2, R_1R_2, and $J(0)$ values and discovered that several residues in the α2-β1 loop (spanning residues 64−78) experience significant enhancements of μs−ms dynamics. In addition, the residues surrounding disulfide-bonded C140 and C172 displayed increased μs−ms dynamics. The disulfide bond has been shown previously to be critical for pilus assembly and stability, and assembled filaments can be rapidly dissociated by reducing agents.[31,32] The notable μs−ms dynamics of the α2-β1 loop suggested that it could also influence pilus assembly or stability.

Involvement of the Pilin's $\alpha\beta$ Loop in Pilus Assembly. To further explore the implications of the increased μs−ms dynamics of the segment from residues 64−78, we used site-directed mutagenesis to examine its role in PilA function. With the objective of shortening this loop while minimally perturbing other key secondary structure elements such as the 4-stranded antiparallel β-sheet, residues 73 only, 72−74, or 71−75 (Figure

DOI: 10.1021/acsinfecdis.7b00229
ACS Infect. Dis. 2018, 4, 936−943

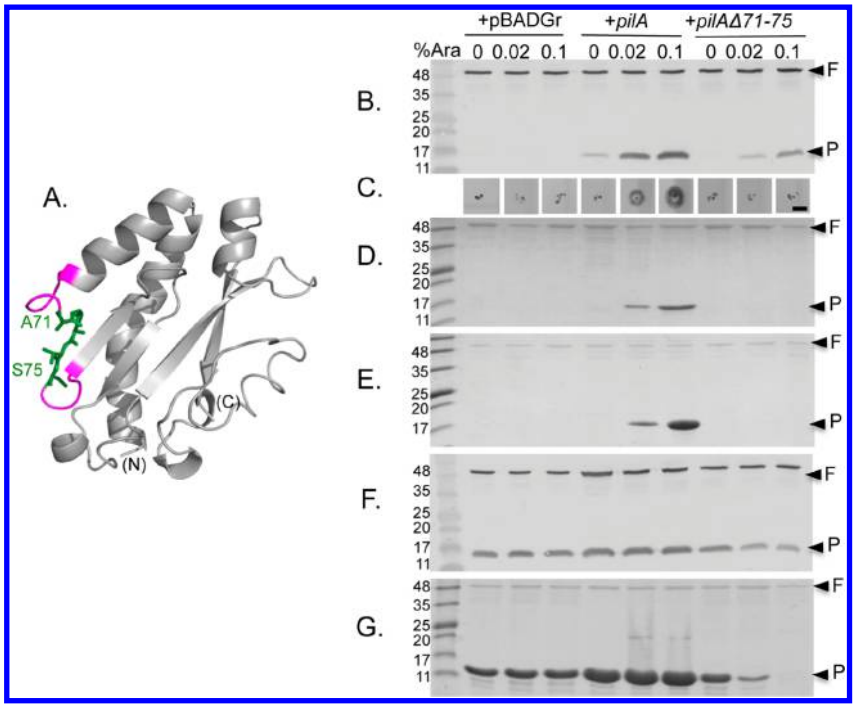

Figure 5. Effects on pilin function of shortening the highly dynamic region of the $\alpha\beta$-loop. (A) Homology model of $PilA_{PA14}$ showing highly dynamic $\alpha\beta$ loop residues 64−78 in magenta and deleted residues 71−75 in green. (B) Western blot of whole cell lysates of the PA14 *pilA* mutant complemented with the vector control (pBADGr), the wild type *pilA* gene, or the Δ71−15 variant, at 0%, 0.02%, or 0.1% L-arabinose. F, flagellin; P, pilin. Molecular weight markers in kDa are on the left. (C) Twitching motility of the strains in panel B. (D) Coomassie-blue stained SDS-PAGE of sheared surface proteins from the strains in panel B. (E) Coomassie-blue stained SDS-PAGE of sheared surface proteins from a PA14 *pilA pilT* double mutant (which is unable to retract any pili that are assembled, trapping them on the cell surface) expressing the same plasmids at the same arabinose concentrations as in panel B. (F) Western blot of whole cell lysates of a PA14 *pilT* mutant (which expresses wild type pilins from the chromosomal locus), complemented with the same constructs at the same arabinose concentrations indicated in panel B. The assembly incompetent mutant pilin leads to a reduction in overall pilin levels as its expression is increased. (G) Coomassie-blue stained SDS-PAGE of sheared surface proteins from the strains in panel F. The mutant pilin has a dose-dependent dominant-negative effect on pilus assembly by the PA14 *pilT* mutant.

5A) were deleted in frame. The wild type and mutant pilin genes were cloned into the arabinose-inducible pBADGr vector and introduced into a PA14 *pilA* mutant to assess the effects of the mutation. For reasons that are not clear, expression of the Δ73 and Δ72−74 pilins in trans caused profound growth defects, while the Δ71−75 variant was well tolerated. Thus, further studies were conducted only with the Δ71−75 construct.

Western blot analysis of whole cell lysates using polyclonal anti-PilA sera verified that, at 0.1% arabinose, the Δ71−75 pilin was present at approximately half of wild type levels, though this could be an underestimate as antibody recognition may be reduced by the deletion (Figure 5B). For the wild type pilin, twitching motility was positively correlated with increasing arabinose concentrations. However, the mutant pilin failed to restore motility at any concentration (Figure 5C). Loss of twitching motility can occur for multiple reasons: complete failure to assemble pili; an imbalance between pilus extension and retraction that results in bald cells; failure to retract assembled pili; or uncoordinated pilus retraction (e.g., retraction at both poles simultaneously) that leads to zero net movement.[33] To distinguish between these possibilities, we examined the level of surface piliation for PA14 *pilA* mutants complemented with wild type or Δ71−75 pilins. Unlike complementation with the wild type gene, complementation with the Δ71−75 pilin failed to restore surface piliation (Figure 5D), consistent with lack of twitching motility.

Assembly failure can be verified by deleting *pilT*, which encodes the retraction ATPase.[16] In that background, any pili that can be assembled, no matter how inefficiently, will be trapped on the cell surface. If no surface pili are recovered in a *pilT* background, we infer that the subunits were incompetent for assembly. We introduced the Δ71−75 pilin construct into a PA14 *pilA pilT* double mutant and tested for surface piliation, which was negative at all concentrations of inducer tested (Figure 5E), showing that the mutant pilin is assembly incompetent. Finally, the same construct was introduced into a PA14 *pilT* single mutant, which produces wild type pilins from the native chromosomal locus (Figure 5F). Interestingly, increasing expression of the assembly incompetent Δ71−75 pilin led to a decrease in the overall levels of intracellular PilA, potentially due to its accumulation in the inner membrane and resulting feedback inhibition on the PilSR two-component system that controls expression of the chromosomal pilin locus.[34] When surface piliation of this strain was tested at various concentrations of inducer, a dose-dependent inhibition of surface piliation was observed, suggesting the Δ71−75 pilin also had a dominant-negative effect on pilus assembly (Figure 5G). In total, these results imply that the region of the protein identified as having high ms−μs dynamics is important for assembly of stable filaments. Dose-dependent disruption of assembly in the *pilT* background might result from a combination of the stochastic incorporation of mutant subunits into growing filaments that disrupts further pilus assembly, and

DOI: 10.1021/acsinfecdis.7b00229
ACS Infect. Dis. 2018, 4, 936−943

decreased expression of assembly competent wild type pilins due to feedback inhibition on their expression.

Many of the functions of T4aP depend on their unique ability to be reversibly assembled and disassembled. This property requires that subunit−subunit interactions be strong enough to withstand pN-scale retraction forces generated during twitching motility[35] yet weak enough that the subunits can be rapidly dissociated at the pilus base to allow the filament to retract.[36] Recent cryo-electron microscopy studies of assembled filaments have reinforced the importance of the networks of hydrophobic interactions in the core of the filament but also revealed that a segment of the α1-N helix between highly conserved P22 and G42 residues becomes unstructured upon polymerization.[37,38] That conformational switch could contribute to the flexibility of the filament but suggests that interactions among other regions of the subunits may contribute to filament stability while that N-terminal segment is remodeled. Our NMR data show that specific loop regions of the pilin exhibit dynamics consistent with a role in protein−protein interactions,[30] and our mutagenesis studies support the hypothesis that such regions may contribute to the formation of stable filaments.

METHODS

Bacterial Strains and Growth Conditions. Bacterial stocks were stored at −80 °C in lysogeny broth (LB) with 15% glycerol. *P. aeruginosa* PA14 and mutants in the PA14 background were grown at 37 °C on LB agar plates supplemented where indicated with gentamicin (30 μg/mL) or carbenicillin (200 μg/mL). *E. coli* strains were grown at 37 °C on LB agar plates supplemented with gentamicin (15 μg/mL) or ampicillin (100 μg/mL).

NMR Sample Preparation. A variant of the PA14 *pilA* gene encoding a 1−28 residue N-terminal truncation of the mature $PilA_{PA14}$ was PCR amplified and cloned into pET151/D-TOPO (Invitrogen) to express $PilA_{PA14}$ with a cleavable N-terminal 6×His-V5 epitope tag. The plasmid was transformed into *E. coli* Origami B (DE3) to allow for formation of a critical C-terminal disulfide bond in PilA, and protein was overexpressed in M9 minimal media with 0.1% ^{15}N-ammonium chloride and 0.3% ^{13}C-glucose. Briefly, a 5 mL LB starter culture was grown for 8 h at 37 °C and then added into 100 mL of M9 media and grown overnight at 37 °C. This overnight culture was added to 900 mL of M9 media and grown to an OD_{600} of 1.0, and protein expression was induced with 0.5 mM IPTG at 20 °C for 22 h. Leucine-selective ^{15}N labeled $PilA_{PA14}$ was also expressed as above except the ammonium chloride was replaced with 0.02% of ^{15}N-labeled leucine and 0.01% of the remaining 19 unlabeled amino acids.

Cells were harvested by centrifugation and lysed by sonication. Purification using nickel affinity chromatography was performed as described previously for $PilA_{0594}$.[24] In brief, the $PilA_{PA14}$ lysate was applied to a nickel affinity chromatography column (GE Healthcare) where His-$PilA_{PA14}$ was eluted with 300 mM imidazole after sequential washes of the column with 25, 40, and 55 mM imidazole. A second nickel affinity purification step was performed following TEV cleavage to remove the histidine and V5 epitope tags, while $PilA_{PA14}$ eluted in the flow through. The flow-through fractions containing purified $PilA_{PA14}$ were pooled, buffer-exchanged into 20 mM Tris, pH 7, 50 mM NaCl and concentrated to 0.5 mM. 5% D_2O was added to the sample for NMR experiments.

NMR Experiments. All data were collected at 33 °C. ^{15}N-^{1}H-HSQC, HN(CO)CA, HNCACB, and CBCA(CO)NH spectra were collected on a Bruker AV spectrometer operating at 700 MHz with a TCI cryoprobe. Additional HNCO, HN(CA)CO, and ^{15}N NOESY-HSQC data were recorded at the Quebec/Eastern Canada High Field NMR Facility on a Varian INOVA spectrometer operating at 500 MHz with a HCN cold probe. NMR data were processed with NMRPipe[39] and analyzed using Sparky.[40] Secondary structure probabilities were calculated on the basis of chemical shifts using PECAN software.[25]

Relaxation Analysis. Transverse (R_2) relaxation rates, acquired at 500 and 800 MHz, were compared with simulated R_2 values from HydroNMR[41] for the PilA homology model. For the HydroNMR simulations, we used an atomic effective radius (AER) of 3.2 Å, an N−H distance of 1.02 Å, and a chemical shift anisotropy of −160 ppm. The temperature and solvent viscosity were set to 306 K and 0.00749 Poises, respectively. Longitudinal (R_1) relaxation rates were also acquired at 500 and 800 MHz and used to compute the R_1R_2 products, which significantly reduce contributions arising from the diffusional anisotropy of the overall tumbling. An approximation of the R_1R_2 product for a rigid rotor model of PilA was obtained by reiteratively averaging the R_1R_2 values and excluding residues outside the average ± one standard deviation from subsequent averages. After three iterations, no further significant changes to the trimmed average R_1R_2 values were observed. Heteronuclear-NOEs, acquired at 800 MHz, were analyzed to probe fast (ps−ns) dynamics in PilA. The R_1, R_2, and HN-NOE values acquired at 800 MHz were also analyzed in terms of reduced spectral densities using approaches described previously.[42−44] An average reduced spectral density at zero frequency (i.e., $J(0)$) value was calculated for all residues, similarly to the R_1R_2 product described above, and used to calculate PilA's correlation time (τ_c). Outliers were detected by plotting lines obtained from the line of best fit and adding or subtracting the corresponding errors from the slope and y-intercept. Any residue, which lies outside this range, was identified as an outlier. Since the slope and intercept errors in the line of best fit obtained for the correlation of theoretical and experimental CB chemical shifts were significantly smaller than those for the CA chemical shifts, we conservatively opted to use the errors from the CA correlation.

Site Directed Mutagenesis of $PilA_{PA14}$. We designed synthetic genes (gBlock, IDT) encoding PA14 PilA with residues 73, 72−74, or 71−75 of the mature pilin (e.g., less its signal sequence) deleted and with flanking *Eco*RI and *Hin*dIII restriction sites for cloning into the corresponding sites of the arabinose-inducible pBADGr vector. The constructs were generated through standard restriction digest and ligation methods, introduced into the PA14 *pilA*, *pilT*, and *pilA pilT* mutants by electroporation, and transformants selected by growth on LB agar plus gentamicin (30 μg/mL) as described previously.[16]

Sheared Surface Protein Isolation and Analysis. Surface proteins were isolated as previously described[11] on LB agar supplemented with gentamicin (30 μg/mL) and L-arabinose (0.02% and 0.1% w/v) to induce protein expression. Samples were separated on 15% SDS-PAGE gels and stained with Coomassie Brilliant Blue for visualization.

Intracellular PilA Protein Levels. Intracellular PilA levels were assessed by Western blot as described previously[16] with minor modifications. Briefly, bacterial cells recovered after

DOI: 10.1021/acsinfecdis.7b00229
ACS Infect. Dis. 2018, 4, 936−943

removal of surface proteins were diluted in 1× PBS to an OD_{600} of 0.6. One milliliter of bacterial suspension was centrifuged at 16 100*g* for 3 min, and the pellets were resuspended in 150 μL of 1× SDS loading buffer and boiled for 10 min. The lysates were separated by SDS-PAGE and transferred to nitrocellulose for immunoblot analysis with polyclonal antisera (1:5000 dilution) raised against sheared pilins and flagellins from strain Pa141123, which is closely related to PA14,[16] and developed using BCIP-NBT. These antisera recognize both PilA and FliC; the latter was used as a loading control. Assays were repeated at least 3 times.

Twitching Motility Assay. Twitching motility stab assays were performed using plasma treated (hydrophilic) 150 mm plates (VWR) with LB 1% agar supplemented with gentamicin (30 μg/mL) and arabinose (0.02%, 0.05%, and 0.1%). After inoculation, plates were incubated at 37 °C for 20 h. The agar was gently removed, and adherent bacteria were stained with 1% (w/v) crystal violet. Twitching zones were photographed and measured using ImageJ. Assays were repeated at least 3 times, with at least 3 replicates per assay.

AUTHOR INFORMATION

Corresponding Author

*Tel.: 905-525-9140 x 22029. E-mail: burrowl@mcmaster.ca.

ORCID

Giuseppe Melacini: 0000-0003-1164-2853

Lori L. Burrows: 0000-0003-0838-5040

Notes

The authors declare no competing financial interest.

ACKNOWLEDGMENTS

This work was supported by a grant from the Canadian Institutes of Health Research (MOP 86639) to L.L.B. Y.N. held CIHR and Cystic Fibrosis Canada Studentships. The 500 MHz NMR experiments were recorded at the Québec/Eastern Canada High Field NMR Facility, supported by the Natural Sciences and Engineering Research Council of Canada, the Canada Foundation for Innovation, the Québec Ministère de la Recherche en Science et Technologie, and McGill University.

REFERENCES

(1) Albers, S. V., and Pohlschroder, M. (2009) Diversity of archaeal type IV pilin-like structures. *Extremophiles 13* (3), 403−410.

(2) Melville, S., and Craig, L. (2013) Type IV pili in Gram-positive bacteria. *Microbiology and Molecular biology reviews: MMBR 77* (3), 323−341.

(3) Pelicic, V. (2008) Type IV pili: e pluribus unum? *Mol. Microbiol. 68* (4), 827−837.

(4) Craig, L., Pique, M. E., and Tainer, J. A. (2004) Type IV pilus structure and bacterial pathogenicity. *Nat. Rev. Microbiol. 2* (5), 363−378.

(5) Ayers, M., Howell, P. L., and Burrows, L. L. (2010) Architecture of the type II secretion and type IV pilus machineries. *Future Microbiol. 5* (8), 1203−1218.

(6) Lyczak, J. B., Cannon, C. L., and Pier, G. B. (2002) Lung infections associated with cystic fibrosis. *Clin. Microbiol. Rev. 15* (2), 194−222.

(7) Murray, T. S., Egan, M., and Kazmierczak, B. I. (2007) *Pseudomonas aeruginosa* chronic colonization in cystic fibrosis patients. *Curr. Opin. Pediatr. 19* (1), 83−88.

(8) Zolfaghar, I., Evans, D. J., and Fleiszig, S. M. (2003) Twitching motility contributes to the role of pili in corneal infection caused by *Pseudomonas aeruginosa*. *Infect. Immun. 71* (9), 5389−5393.

(9) Hahn, H. P. (1997) The type-4 pilus is the major virulence-associated adhesin of *Pseudomonas aeruginosa*−a review. *Gene 192* (1), 99−108.

(10) Nguyen, Y., Harvey, H., Sugiman-Marangos, S., Bell, S. D., Buensuceso, R. N., Junop, M. S., and Burrows, L. L. (2015) Structural and functional studies of the *Pseudomonas aeruginosa* minor pilin, PilE. *J. Biol. Chem. 290* (44), 26856−26865.

(11) Nguyen, Y., Sugiman-Marangos, S., Harvey, H., Bell, S. D., Charlton, C. L., Junop, M. S., and Burrows, L. L. (2015) *Pseudomonas aeruginosa* minor pilins prime type IVa pilus assembly and promote surface display of the PilY1 adhesin. *J. Biol. Chem. 290* (1), 601−611.

(12) Heiniger, R. W., Winther-Larsen, H. C., Pickles, R. J., Koomey, M., and Wolfgang, M. C. (2010) Infection of human mucosal tissue by *Pseudomonas aeruginosa* requires sequential and mutually dependent virulence factors and a novel pilus-associated adhesin. *Cell. Microbiol. 12* (8), 1158−1173.

(13) Nunn, D. N., and Lory, S. (1991) Product of the *Pseudomonas aeruginosa* gene *pilD* is a prepilin leader peptidase. *Proc. Natl. Acad. Sci. U. S. A. 88* (8), 3281−3285.

(14) Kus, J. V., Tullis, E., Cvitkovitch, D. G., and Burrows, L. L. (2004) Significant differences in type IV pilin allele distribution among *Pseudomonas aeruginosa* isolates from cystic fibrosis (CF) versus non-CF patients. *Microbiology (London, U. K.) 150* (5), 1315−1326.

(15) Harvey, H., Bondy-Denomy, J., Marquis, H., Sztanko, K., Davidson, A. R., and Burrows, L. L. (2018) *Pseudomonas aeruginosa* defends against phages through type IV pilus glycosylation. *Nature Microbiology 3* (1), 47−52.

(16) Asikyan, M. L., Kus, J. V., and Burrows, L. L. (2008) Novel proteins that modulate type IV pilus retraction dynamics in Pseudomonas aeruginosa. *J. Bacteriol. 190* (21), 7022−7034.

(17) Audette, G. F., Irvin, R. T., and Hazes, B. (2004) Crystallographic analysis of the *Pseudomonas aeruginosa* strain K122−4 monomeric pilin reveals a conserved receptor-binding architecture. *Biochemistry 43* (36), 11427−11435.

(18) Craig, L., Taylor, R. K., Pique, M. E., Adair, B. D., Arvai, A. S., Singh, M., Lloyd, S. J., Shin, D. S., Getzoff, E. D., Yeager, M., Forest, K. T., and Tainer, J. A. (2003) Type IV pilin structure and assembly: X-ray and EM analyses of *Vibrio cholerae* toxin-coregulated pilus and *Pseudomonas aeruginosa* PAK pilin. *Mol. Cell 11* (5), 1139−1150.

(19) Hazes, B., Sastry, P. A., Hayakawa, K., Read, R. J., and Irvin, R. T. (2000) Crystal structure of *Pseudomonas aeruginosa* PAK pilin suggests a main-chain-dominated mode of receptor binding. *J. Mol. Biol. 299* (4), 1005−1017.

(20) Keizer, D. W., Slupsky, C. M., Kalisiak, M., Campbell, A. P., Crump, M. P., Sastry, P. A., Hazes, B., Irvin, R. T., and Sykes, B. D. (2001) Structure of a pilin monomer from *Pseudomonas aeruginosa*: implications for the assembly of pili. *J. Biol. Chem. 276* (26), 24186−24193.

(21) Wiehlmann, L., Wagner, G., Cramer, N., Siebert, B., Gudowius, P., Morales, G., Kohler, T., van Delden, C., Weinel, C., Slickers, P., and Tummler, B. (2007) Population structure of *Pseudomonas aeruginosa*. *Proc. Natl. Acad. Sci. U. S. A. 104* (19), 8101−8106.

(22) Dunlop, K. V., Irvin, R. T., and Hazes, B. (2005) Pros and cons of cryocrystallography: should we also collect a room-temperature data set? *Acta Crystallogr., Sect. D: Biol. Crystallogr. 61* (1), 80−87.

(23) Giltner, C. L., Nguyen, Y., and Burrows, L. L. (2012) Type IV pilin proteins: versatile molecular modules. *Microbiol Mol. Biol. Rev. 76* (4), 740−772.

(24) Nguyen, Y., Jackson, S. G., Aidoo, F., Junop, M., and Burrows, L. L. (2010) Structural characterization of novel *Pseudomonas aeruginosa* type IV pilins. *J. Mol. Biol. 395* (3), 491−503.

(25) Eghbalnia, H. R., Wang, L., Bahrami, A., Assadi, A., and Markley, J. L. (2005) Protein energetic conformational analysis from NMR chemical shifts (PECAN) and its use in determining secondary structural elements. *J. Biomol. NMR 32* (1), 71−81.

(26) Sharma, D., and Rajarathnam, K. (2000) 13C NMR chemical shifts can predict disulfide bond formation. *J. Biomol. NMR 18* (2), 165−171.

DOI: 10.1021/acsinfecdis.7b00229
ACS Infect. Dis. 2018, 4, 936−943

(27) Kelley, L. A., Mezulis, S., Yates, C. M., Wass, M. N., and Sternberg, M. J. (2015) The Phyre2 web portal for protein modeling, prediction and analysis. *Nat. Protoc. 10* (6), 845−858.
(28) Neal, S., Nip, A. M., Zhang, H., and Wishart, D. S. (2003) Rapid and accurate calculation of protein 1H, 13C and 15N chemical shifts. *J. Biomol. NMR 26* (3), 215−240.
(29) Williamson, M. P. (2013) Using chemical shift perturbation to characterise ligand binding. *Prog. Nucl. Magn. Reson. Spectrosc. 73*, 1−16.
(30) Feher, V. A., and Cavanagh, J. (1999) Millisecond-timescale motions contribute to the function of the bacterial response regulator protein Spo0F. *Nature 400* (6741), 289−293.
(31) Harvey, H., Habash, M., Aidoo, F., and Burrows, L. L. (2009) Single-residue changes in the C-terminal disulfide-bonded loop of the *Pseudomonas aeruginosa* type IV pilin influence pilus assembly and twitching motility. *J. Bacteriol. 191* (21), 6513−6524.
(32) Li, J., Egelman, E. H., and Craig, L. (2012) Structure of the *Vibrio cholerae* Type IVb Pilus and stability comparison with the *Neisseria gonorrhoeae* type IVa pilus. *J. Mol. Biol. 418* (1−2), 47−64.
(33) Burrows, L. L. (2012) *Pseudomonas aeruginosa* twitching motility: type IV pili in action. *Annu. Rev. Microbiol. 66*, 493−520.
(34) Kilmury, S. L., and Burrows, L. L. (2016) Type IV pilins regulate their own expression via direct intramembrane interactions with the sensor kinase PilS. *Proc. Natl. Acad. Sci. U. S. A. 113* (21), 6017−6022.
(35) Maier, B., Potter, L., So, M., Long, C. D., Seifert, H. S., and Sheetz, M. P. (2002) Single pilus motor forces exceed 100 pN. *Proc. Natl. Acad. Sci. U. S. A. 99* (25), 16012−16017.
(36) McCallum, M., Tammam, S., Khan, A., Burrows, L. L., and Howell, P. L. (2017) The molecular mechanism of the type IVa pilus motors. *Nat. Commun. 8*, 15091.
(37) Kolappan, S., Coureuil, M., Yu, X., Nassif, X., Egelman, E. H., and Craig, L. (2016) Structure of the *Neisseria meningitidis* Type IV pilus. *Nat. Commun. 7*, 13015.
(38) Wang, F., Coureuil, M., Osinski, T., Orlova, A., Altindal, T., Gesbert, G., Nassif, X., Egelman, E. H., and Craig, L. (2017) Cryoelectron Microscopy Reconstructions of the *Pseudomonas aeruginosa* and *Neisseria gonorrhoeae* Type IV Pili at Sub-nanometer Resolution. *Structure 25* (9), 1423−1435.e4.
(39) Delaglio, F., Grzesiek, S., Vuister, G. W., Zhu, G., Pfeifer, J., and Bax, A. (1995) NMRPipe: a multidimensional spectral processing system based on UNIX pipes. *J. Biomol. NMR 6* (3), 277−293.
(40) Goddard, T. D., and Kneller, D. G. *SPARKY 3*, University of California, San Francisco.
(41) Garcia de la Torre, J., Huertas, M. L., and Carrasco, B. (2000) HYDRONMR: prediction of NMR relaxation of globular proteins from atomic-level structures and hydrodynamic calculations. *J. Magn. Reson. 147* (1), 138−146.
(42) Das, R., Chowdhury, S., Mazhab-Jafari, M. T., Sildas, S., Selvaratnam, R., and Melacini, G. (2009) Dynamically driven ligand selectivity in cyclic nucleotide binding domains. *J. Biol. Chem. 284* (35), 23682−23696.
(43) Das, R., Mazhab-Jafari, M. T., Chowdhury, S., SilDas, S., Selvaratnam, R., and Melacini, G. (2008) Entropy-driven cAMP-dependent allosteric control of inhibitory interactions in exchange proteins directly activated by cAMP. *J. Biol. Chem. 283* (28), 19691−19703.
(44) Boulton, S., Akimoto, M., Akbarizadeh, S., and Melacini, G. (2017) Free energy landscape remodeling of the cardiac pacemaker channel explains the molecular basis of familial sinus bradycardia. *J. Biol. Chem. 292* (15), 6414−6428.

DOI: 10.1021/acsinfecdis.7b00229
ACS Infect. Dis. 2018, 4, 936−943